International Journal of Chemical and Biochemical Sciences
(ISSN 2226-9614)

Journal Home page: www.iscientific.org/Journal.html

Electrochemical and Quantum Chemical Investigations of novel pyrazole derivatives as a Corrosion Inhibitor for Stainless Steel in 2M H_2SO_4 medium

Hoyam CHAHMOUT[1]; Moussa OUAKKI[1,2]; Sarra SIBOUS[1]; Elhachmia ECH-CHIHBI[3,4]; Zakaria BENZEKRI[1,5]; Saïd BOUKHRIS[1]; Abdelaziz SOUIZI[1]; Mohammed CHERKAOUI[1,2]*

[1] *Laboratory of Organic Chemistry, catalysis and Environment, Faculty of Sciences, Ibn Tofaïl University, PO Box 133, 14000, Kenitra, Morocco*
[2] *National Higher School of Chemistry, Ibn Tofail University, PB 133-14050 Kénitra, Morocco*
[3] *Euro-Mediterranean University of Fes, Fez, Morocco*
[4] *Engineering Laboratory of Organometallic, Molecular Materials, Environment, Faculty of Sciences, University Sidi Mohamed Ben Abdellah, Fez, Morocco*
[5] *laboratory of heterocyclic organic chemistry, department of chemistry, faculty of sciences, Mohammed V university in Rabat, BP, 1014, Rabat, Morocco.*

Abstract

Stainless steels play a crucial role in diverse industrial domains. However, due to their exposure to acidic environments, stainless steels undergo the corrosion phenomenon, leading to the deterioration of the material and its properties. Thus, the objective of this work is to study the corrosion inhibition of stainless steel in an H_2SO_4 2M medium by using two organic compounds, namely Py-3:{1-amino-5,10-dioxo-3-(p-tolyl)-5,10-dihydro-1H-pyrazolo[1,2-b] phthalazine-2-carbonitrile} and Py-4:{1-amino-3-(2-chlorophenyl)-5,10-dioxo-5,10-dihydro-1H-pyrazolo[1,2-b]phthalazine-2carbonitrile}. This study was conducted using transient electrochemical methods in conjunction with a theoretical approach. The obtained results demonstrate that the addition of pyrazole compounds in the corrosive medium H_2SO_4 exhibits excellent inhibitory power against steel corrosion, with an inhibitory efficiency reaching 98%. The tested inhibitors are adsorbed into the surface of the metal by chemical bonds, Moreover, the adsorption of these compounds follows the Langmuir adsorption model. Theoretical calculations based on the Density Functional Theory (DFT) provide a better understanding of the reactivity of tested inhibitor towards stainless steel which they are in good agreement with the experimental findings.

Keywords: corrosion, stainless steel, inhibition, pyrazole, EIS, DFT

Full length article **Corresponding Author*, e-mail: moussa.ouakki@uit.ac.ma Doi # https://doi.org/10.62877/10-IJCBS-24-25-19-10

1. Introduction

Corrosion of materials is a pressing problem that requires significant attention and rapid understanding within the scientific community. Despite modern technological developments, it remains the main issue in many works, because it remains a problem that is often difficult to eliminate. The consequences of corrosion can cause irreversible damage to the environment and even to human life. One of the serious consequences of corrosion involves economic losses, with industrialized countries recording a loss of around 3 to 4% of their gross national product (GNP) [1]. However, of the total cost, 20 to 25% of losses can be saved by a better understanding of the causes of corrosion and better application of protection techniques. Due to their excellent mechanical properties, stainless steels play an important role in a wide range of sectors, including the chemical, petrochemical, and pharmaceutical industries [2]. However, due to their interactions with the environment, stainless steels undergo the phenomenon of corrosion, resulting in material deterioration and the loss of their properties. Several methods of corrosion protection have been considered so far [3-6]. These techniques can be

classified into two main categories: those that act on the metal such as metallic or organic coatings, the use of a more noble material, cathodic and anodic protection [7,8], on the other hand those that modify the aggressiveness of the environment as the use of organic inhibitors. Utilizing corrosion inhibitors is regarded as the most effective strategy for protecting materials against corrosion, due to their low cost, ease of application, and high effectiveness [9,10]. Organic molecules containing heteroatoms such as N, S, O, or P, π-conjugated systems, or compounds with aromatic rings are frequently used to control metal corrosion in acidic environments. The ability of organic compounds to inhibit corrosion derives from their adsorption to the metal surface by two main types of interaction, namely physical adsorption, and chemisorption [11-13]. In this context, several tests have been conducted on various organic compounds such as triazole derivatives [14], pyrrole [15], benzothiazine [16], and hydrazine [17], which have shown significant inhibitory effectiveness against corrosion in acidic environments. Recently, pyrazole and its derivatives have been regarded as an important class of anticorrosive compounds, especially in acidic solutions [18-20], due to their strong adsorption capacity. This group of organic compounds is frequently linked to various biological activities, such as antimicrobial, antifungal, antitubercular, anti-inflammatory, anticonvulsant, anticancer, and antiviral properties [21]. The objective of this study is to assess the inhibitory effects of two pyrazole compounds namely Py-3:{1-amino-5,10-dioxo-3-(p-tolyl)-5,10-dihydro-1H pyrazolo[1,2-b]phthalazine-2-carbonitrile} and Py-4:{1-amino-3-(2-chlorophenyl)-5,10-dioxo-5,10-dihydro-1H-pyrazolo[1,2-b]phthalazine-2carbonitrile} in a 2M H_2SO_4 solution using transient electrochemical techniques based on electrochemical impedance spectroscopy. Additionally, a theoretical investigation of the molecules understudy was carried out using density functional theory (DFT) methods to enhance our understanding of how the inhibitory molecules interact with the surface of the steel. The theoretical calculation of both global and local quantum reactivity descriptors (E_{HOMO}, E_{LUMO}, μ, χ, η, ΔN, and the Fukui index) offers valuable insights into the adsorption mechanism of the inhibitors under investigation and identify sites that are particularly reactive to nucleophilic and/or electrophilic attacks.

2. Materials and Methods

2.1. Materials and corrosive medium

The corrosive medium is 2M sulfuric acid (H_2SO_4) solution, prepared by diluting concentrated commercial acid at 98% with distilled water. The material under examination is stainless steel, with its elemental composition by mass fraction detailed in Table 1. The steel specimen takes the shape of a plate, providing a contact surface area with an electrolyte of approximately 1cm^2. Before each test, the stainless-steel samples are prepared by polishing with abrasive paper of increasing grit size (from 200 to 2000 grade). Following this, they are rinsed with distilled water and finally dried. The chemical structure of the two compounds under examination (Py-3 and Py-4) is depicted in Figure 1. These compounds were dissolved in 2 ml of dimethyl sulfoxide (DMSO), with the concentration of the inhibitors varying from 10^{-6} to 10^{-3} M.

2.2. Electrochemical study

Electrochemical experiments were conducted employing a standard three-electrode setup in a Pyrex glass cell. The reference electrode utilized was a silver chloride electrode (Ag/AgCl), while a platinum plate served as the counter electrode. For the working electrode, stainless steel with a surface area of 1cm^2 was employed. Polarization and impedance tests were conducted using a PGZ100 Potentiostat/Galvanostat/Voltalab under the control of a computer equipped with Volta Master 4 software. Before each measurement, the working electrode was immersed in the test solution for 30 minutes at the open-circuit potential to stabilize the system at a corrosion potential [22]. Electrochemical impedance measurements were conducted across a frequency range spanning from 100 kHz to 10 mHz, applying a sinusoidal perturbation potential with an amplitude of 10 mV. The corrosion inhibition efficiency (η_{imp}%) is deduced from the charge transfer resistance (R_{ct}) values, utilizing the following equation [23]:

$$\eta_{imp}\% = (R_{tc} - R_{tc}^{\circ}/R_{tc}) \times 100$$
$$\theta = R_{tc} - R_{tc}^{\circ}/R_{tc}$$

With R_{tc}° and R_{tc} are the charge transfer resistance in the absence and presence of an inhibitor, respectively, and θ is the recovery rate.

2.3. Computational methodology

To support the preceding findings, a Density Functional Theory (DFT) investigation was conducted on both the neutral and protonated forms of Py1 and Py2 in a solution phase. The study utilized the commonly employed B3LYP functional and the 6–311G (d,p) basis set, employing the Gaussian 09W program package and GaussView 5.0 program . In this study, all computations were carried out using the IEFPCM method to simulate a water solution environment. The energies of E_{HOMO} and E_{LUMO} orbitals, the energy gap (ΔEL-H), along with other quantum chemical descriptors, were predicted to explore the relationship between the experimentally obtained inhibition efficiencies and the molecular structures of the investigated compounds.

3. Results and discussion

3.1. Electrochemical impedance spectroscopy

Electrochemical Impedance Spectroscopy (EIS) stands out as a reliable method for investigating the surface properties of steel samples and the dynamics of charge transfer occurring at the interface between the electrolyte and the electrode. The impedance diagrams obtained provide access to the values of physical parameters characterizing the system (Rs, Rtc, Cdc, n...), and thus, to the inhibitory efficiency rate under the experimental conditions used. The analysis of electrochemical parameters derived from impedance diagrams provides insights into the corrosion process mechanism and also serves as quantitative means to compare the performance of different components of the system. The impedance diagrams of stainless steel immersed in the corrosive solution of 2M H_2SO_4, with and without the

addition of inhibitors Py-3 and Py-4 at various concentrations, are presented as Nyquist plots in Figure 2 and as Bode plots in Figure 4. The diagrams obtained in the 2M H_2SO_4 medium without inhibitor consist of two capacitive loops: the first one at high frequency is attributed to the relaxation process within the natural oxide present on the surface of the sample and its dielectric properties, while the second one at low frequency is attributed to the charge transfer process [24, 25]. The Nyquist diagrams obtained exhibit a similar appearance after adding the pyrazole compounds to the aggressive solution. They are characterized by two capacitive loops: one at high frequency attributed to the adsorption of a film formed by inhibitor molecules, and the other at low frequency attributed to the charge transfer resistance. Additionally, we observe that the size of the loop gradually increases with the addition of different concentrations of tested inhibitors [26]. This result reflects the effect of the inhibitor on the dissolution process of stainless steel in a 2M H_2SO_4 environment. Additionally, we can observe that the impedance plots obtained do not form perfect semicircles. This deviation is attributed to the frequency dispersion of interfacial impedance [27-29], this phenomenon typically stemming from the heterogeneity of the electrode surface. This heterogeneity could be caused by various factors including surface roughness, impurities, dislocations, inhibitor adsorption, and the formation of porous layers [30, 31]. The electrochemical impedance spectroscopy (EIS) data were analyzed using the EC-lab software to simulate equivalent electrical circuits, as illustrated in Figure 3. The suggested equivalent circuit includes the following components: Rs represents the solution resistance, R_{tc} the charge transfer resistance, R_f the film resistance, and Q_f and Q_{tc} the elements with constant phase [32]. All impedance spectra obtained from the exposed steel electrode for 30 minutes in 2M H_2SO_4 solutions containing the studied inhibitors were analyzed using the equivalent circuit shown in Figure 3. As can be seen in Figure 3, the capacitor has been replaced by a constant phase element with a fractional exponent n, indicating the presence of a dissimilar frequency response. The CPE impedance is defined as follows [33]:

$$Z_{CPE}(\omega) = Q^{-1}(j\omega)^{-n}$$

With Q expressed in units of $\Omega.cm^{-2}.s^n$, ω denoting the angular frequency in rad s^{-1}($\omega = 2\pi f_{max}$), f_{max} representing the frequency at the peak of the semicircle, n is the empirical exponent of the CPE, measuring the deviation from ideal capacitive behavior. This parameter can be used as an indicator of surface heterogeneity or roughness, with $-1 < n < 1$. ZCPE can represent an inductance (n = -1), a Warburg impedance (n = 0.5), a pure capacitance (n = 1), or a resistance (n = 0). Thus, it is observed that the smaller the value of n, the higher the surface roughness [34,35]. The electrochemical parameters obtained from the impedance diagrams are grouped in Table 2. These parameters include the film resistance (R_f), charge transfer resistance (R_{tc}), polarization resistance (R_p), constant phase elements (Q_i), and inhibitory efficiency η_{imp}%. The values of the polarization resistance (R_p) for all systems are calculated using the following equation:

$$R_p = R_f + R_{tc}$$

The corrosion inhibitory efficiency of the steel is calculated from the charge transfer resistance using the following relation:

$$\eta_{imp}\% = \frac{R_{tc} - R_{tc}^0}{R_{tc}} \times 100$$

Where R_{tc}^0 and R_{tc} are respectively the values of the charge transfer resistances of the steel in the absence and presence of the inhibitor. The analysis of the results regrouped in Table 2 reveals that the values of Q_f decrease and the polarization resistance increases with the concentrations of the studied inhibitors. The decrease in Q_f may result from a local decrease in the dielectric constant and/or an increase in the thickness of the double layer. This has been attributed to the gradual replacement of water molecules and other ions initially adsorbed on the surface by the adsorption of inhibitor molecules on the metal surface [36-38]. However, the increase in the coefficient (n_f and n_{tc}) with inhibitor concentration reflects the decrease in surface heterogeneity of the stainless steel, which results from the adsorption of inhibitor molecules onto the steel surface. Furthermore, the values of these parameters are close to unity ($n \simeq 1$) for all inhibited systems, implying that the double layer between the charged metal surface and the solution is considered an electrical capacitor whose capacity decreases due to the adsorption of inhibitor molecules onto the steel surface, thus forming a protective layer that reduces the number of active corrosion sites [39]. According to the Helmholtz model, the capacitance of the double layer C_{dc} is calculated by the following equation [40, 41]:

$$C_{dc} = \frac{\varepsilon \varepsilon_0 S}{e}$$

Where e is the thickness of the deposit; ε is the dielectric constant; ε_0 is the permittivity of the medium (8.854×10^{-14} F cm^{-1}), and S is the surface area of the electrode. The inhibitory efficiency (η_{imp}%) rises as inhibitor concentrations increase, leading to higher R_p values, which indicate improved inhibition efficiency due to enhanced adsorption of inhibitor molecules on the steel surface. These findings have been fully explained by numerous authors [42, 43]. The Bode spectrum obtained for steel in the absence and presence of inhibitors Figure 4 shows two maximum phases at low and high frequencies, indicating the detection of two-time constants. These results confirm the equivalent electrical circuit model used to simulate the experimental data. The values of the impedance modulus log (|Z|) in the low-frequency region are used to prove the performance of the tested compounds as corrosion inhibitors. As can be seen in Figure 4, the increasing values of log (|Z|) indicate that corrosion resistance is very high, and that the inhibitors tested are good inhibitors with high inhibitory efficiency [44]. Consequently, the results obtained in Figure 4 show that log (|Z|) values at low frequencies are greater for the Py-3 inhibitor. This confirms the better performance of this compound. The phase angle values obtained for steel in the presence of inhibitors are higher than those obtained in the absence of inhibitors. As inhibitor concentration increases, phase angle values increase up to 70°. This suggests that inhibited samples have a lower

surface roughness, reflecting a higher inhibition behavior attributed to inhibitor adsorption on the stainless-steel surface [45,46].

3.2. Adsorption isotherms

The corrosion inhibition of metals by organic compounds is explained by their adsorption on the metal surface. This is described by two main types of adsorptions: physical adsorption and chemical adsorption. It depends on the charge of the metal, its nature, the chemical structure of the organic product, and the type of electrolyte. Indeed, in an aqueous solution, the adsorption at the metal-solution interface of organic molecules coming from the solution is generally accompanied by the desorption of water molecules already adsorbed on the metal surface. This adsorption is therefore considered as a substitutional adsorption phenomenon, as shown by the following reaction [47]:

$$Org_{aq} + xH_2O_{ads} \leftrightarrow Org_{ads} + xH_2O_{aq}$$

Org_{aq} and Org_{ads} are respectively the organic molecules in solution and adsorbed on the stainless-steel surface, x denotes the number of water molecules replaced by the inhibitor molecule. There are several types of adsorption isotherms used to evaluate the adsorption phenomenon on the metal surface. Among the most commonly used isotherms are: Langmuir, Temkin, Frumkin, and Freundlich. According to these adsorption isotherms, the coverage rate is related to the inhibitor concentration according to the equations illustrated in the following table 3. The Figure 5 below represents the Langmuir isotherm. According to our study, the Langmuir adsorption isotherm shows an excellent fit with the experimental values, implying that it appears to be the most suitable to describe the adsorption of Py-3 and Py-4 inhibitors on the stainless-steel surface. This model assumes that the steel surface has a fixed number of adsorption sites, and that each site can accommodate only one adsorbed species. Furthermore, there is no interaction between adsorbed molecules, and all adsorption sites are thermodynamically equivalent. Thus, the adsorption energy does not depend on the surface coverage rate θ, which means that the adsorption energy is constant for all sites [55,56]. The adsorption constant K_{ads} is related to the standard free energy of adsorption ΔG_{ads} by the following equation [57]:

$$K_{ads} = \frac{1}{55.5} e^{-\frac{\Delta G_{ads}}{RT}}$$

Where 55.5 is the molar concentration of water (mol/l), R is the universal gas constant and T is the absolute temperature. The calculated thermodynamic parameters are shown in Table 4. According to the data in the table, we observed a high correlation coefficient (R^2) for the two products, and the slope is very close to unity. These results indicate that the experimental data are well described. The high K_{ads} values for the two compounds tested indicate their strong adsorption to the steel surface (Table 4). This can be simply explained by the presence of several donor atoms, such as oxygen, nitrogen and chlorine, in the functional groups of the molecules. The negative values of ΔG_{ads} are compatible with the spontaneity of the adsorption process and the stability of the adsorbed layer on the steel surface. In general, absolute values of ΔG_{ads} close to -20 kj.mol^{-1} are associated with electrostatic interactions between the charged molecules and the charged metal (physical adsorption), while those approaching -40 kj.mol^{-1} suggest electron sharing or transfer between the active sites of the inhibitor and the vacant "d" orbitals of the metal, with a coordination bond being formed (covalent bond), thus indicating chemisorption [58-60]. The standard free energy of adsorption ΔG_{ads} calculated for the Py-3 and Py-4 inhibitors are close to -40 Kj.mol^{-1}. This indicates that the adsorption of our inhibitors on the steel surface is of the chemical type.

3.3. Quantum calculations

Theoretical chemistry has been increasingly successful due to its ability to provide results and explanations that are not accessible through experimental approaches alone. Currently, DFT is very popular because it can handle large systems, including electronic correlation effects [61]. In this study, theoretical calculations of various parameters were conducted based on Density Functional Theory (DFT) at the B3LYP/6–311G (d,p) basis set implemented in the Gaussian 09 software [62]. The DFT method is used in an aqueous environment to correlate the results of experimental studies and to establish a relation between inhibition efficiencies and the structure of inhibitor molecules. The optimized structures of the studied pyrazole molecules in their neutral state (Py-3 and Py-4) in an aqueous environment are presented in Figure 6. The presence of heteroatoms in the studied molecules promotes their strong tendency to protonate in acidic solution [63]. Therefore, the percentage of observed species as a function of the pH diagrams of the Py-3 and Py-4 molecules using the MarvinSketch software is presented in Figure 6 [64]. Figure 6 clearly shows that the mono-protonated forms both studied species in N14 are the most favored and stable at a pH close to 0. The optimized structures of the protonated pyrazole molecules are illustrated in Figure 6. The properties of neutral and protonated molecules such as the highest occupied molecular orbital (HOMO), lowest unoccupied molecular orbital (LUMO), energy gap, dipole moment, and other quantum parameters are calculated and correlated with the inhibitory efficiencies of the molecules. From Figure 7, the HOMO electron density distribution shows that the electron-donating adsorption centers for both systems are localized on the pyrazolo-pyridazine and heteroatom moiety regions. However, the electron density of LUMO also extends over the same regions as HOMO, but in this case the C13-linked phenyl ring is also involved. In the case of protonated species, the HOMO densities of the molecules studied appeared less dense than those of neutral forms, with significant localization on the phenyl ring. The molecular electrostatic potential (MEP) is a descriptor directly linked to electron density used to predict active sites and their reactivity to electrophilic and nucleophilic attacks [65]. The regions of molecular electrostatic potential (MEP) of the inhibitors studied were calculated and presented in Figure 7. Different values of electrostatic potential are represented by different colors. The potential increases in the order red, orange, yellow, green, blue. The negative regions of the MEP (red and yellow) are linked to electrophilic reactivity, while the positive electron density found in the blue regions is generally associated with nucleophilic reactivity. In our case, the MEP

of both pyrazole molecules shows that the most negative region is distributed mainly near the oxygen atoms. Figure 7 clearly shows that the electrophilic regions (represented by the color blue) cover the entire molecular surface of the compounds studied, indicating that these regions are electron-deficient and also confirming their very low tendency to donate electrons. In order to correlate the anti-corrosion activity obtained experimentally with the structural and electronic properties of the two neutral and protonated inhibitor molecules and to interpret their adsorption mode on the metal surface, we calculated a number of electronic descriptors such as the highest occupied molecular orbital energy (EHOMO), the lowest unoccupied molecular orbital energy (E_{LUMO}), the energy gap ($E_{HOMO} - E_{LUMO}$), the electronegativity (χ), the global hardness (η), the global softness (σ), and the dipole moment (μ). The results are presented in Table 5. Quantum molecular descriptors are calculated using the following equations [66,67]:

$$\Delta E_{gap} = E_{LUMO} - E_{HOMO}$$

$$\eta = \frac{\Delta E_{gap}}{2} = \frac{\left(E_{LUMO} - E_{HOMO}\right)}{2}$$

$$\sigma = \frac{1}{\eta} = \frac{2}{E_{LUMO} - E_{HOMO}}$$

The fraction of electrons transferred (ΔN110) is determined using the following formula:

$$\Delta N = \frac{\Phi - \chi_{inh}}{2\left(\eta_{Fe_{110}} + \eta_{inh}\right)}$$

Where the work function value Φ used in this study is 4.82 eV on the (110) lattice plane of Fe. [68]. The higher HOMO energy value (E_{HOMO}) is linked to greater corrosion inhibition efficiency due to the higher electron donation potential of the inhibitor centers of the molecule under study towards the unoccupied d orbital of the steel surface [69,70].

Generally, the smallest value of E_{LUMO} is attributed to the high electron-accepting potential of the inhibitor molecule, which is responsible for its high inhibition performance, meaning that this molecule can easily accept electrons from the unoccupied d orbital of the metal surface [71]. The largest energy band gap ($E_{HOMO} - E_{LUMO}$) indicates lower reactivity and interaction between the two molecular frontier orbitals, HOMO and LUMO [72]. Therefore, the Py-3 molecule has higher stability and reactivity than the Py-4 molecule, indicating that Py-3 has a stronger donating effect than the Py-4 molecule:

$$\Delta E \text{ (Py-3)} < \Delta E \text{ (Py-4)}$$

Many studies have reported that molecules with high polarity exhibit higher reactivity than those with low polarity. In this study, the correlation between the dipole moment and the inhibition efficiency of the two studied molecules shows that inhibition decreases with polarity. The positive values obtained for ΔN for the neutral state molecules indicate that these inhibitor forms tend to transfer their electrons to the vacant d orbitals of Fe atoms during interactions between the inhibitors and the metals. However, for the protonated forms, the negative sign of ΔN for the molecules indicates the transfer of electrons from the vacant d orbitals of Fe atoms to the protonated inhibitors during interactions with the metallic inhibitors. Furthermore, it is noted that for the protonated forms (Table 5), the compound Py-3 exhibits the smallest hardness value and a higher softness value for both protonated and neutral forms studied, confirming the most significant inhibitory power of this molecule compared to Py-4 compounds. All quantum chemistry descriptors indicate that the neutral form of the two studied inhibitors has better adsorption properties and could be the stable form of these molecules in the aqueous phase.

3.4. Fukui Functions

The reactive sites that likely contribute to the adsorption of pyrazole molecules on the metal were studied using Fukui functions. The Fukui function is one of the local density-dependent selectivity descriptors widely used to model the chemical reactivity of different sites on a molecule [73]. These descriptors (fk+ and fk-) indicate the reactive centers of the molecules (nucleophilic and electrophilic centers). Generally, f_k^+ measures the changes in density when molecules gain electrons and corresponds to reactivity towards nucleophilic attack. On the other hand, f_k^- corresponds to reactivity towards electrophilic attack when the molecule loses electrons. Nucleophilic and electrophilic attacks are controlled by the maximum values of fk^+ and fk^-. The Fukui functions, which represent the indices of attacks of nucleophilic and electrophilic centers, using Mulliken population analysis (NPA), are calculated as follows [74,13]:

Attacks of nucleophilic centers: $f_k^+ = P_k(N+1) - P_k(N)$

Attacks of electrophilic centers: $f_k^- = P_k(N) - P_k(N-1)$

Where P_k (N), P_k (N + 1), and P_k (N-1), are the neutral, anionic, and cationic Mulliken populations of an atom k in an inhibitor molecule, respectively. The Fukui indices for the molecules studied in the aqueous phase have been graphically represented in Figure 8. According to the Fukui index calculations presented in Figure 8, it can be observed that for all studied inhibitors, the highest values of fk+ and fk- are distributed over the regions of the pyrazolo-pyridazine moiety, chlorine atoms, as well as various nitrogen and oxygen heteroatoms. These regions exhibit significant nucleophilic and electrophilic characteristics. These atoms are thus the preferred sites that release electrons when targeted by a nucleophilic reagent. Therefore, all these sites in the studied molecules could be responsible for the inhibition efficiency.

Table 1. Chemical composition of stainless steel

Elements	Fe	C	Si	Mn	P	S	N	Cr	Co	Mo	Ni	Cu
%	Bal	0.04	0.41	1.46	0.07	0.03	0.08	18.5	0.16	0.33	7.81	0.51

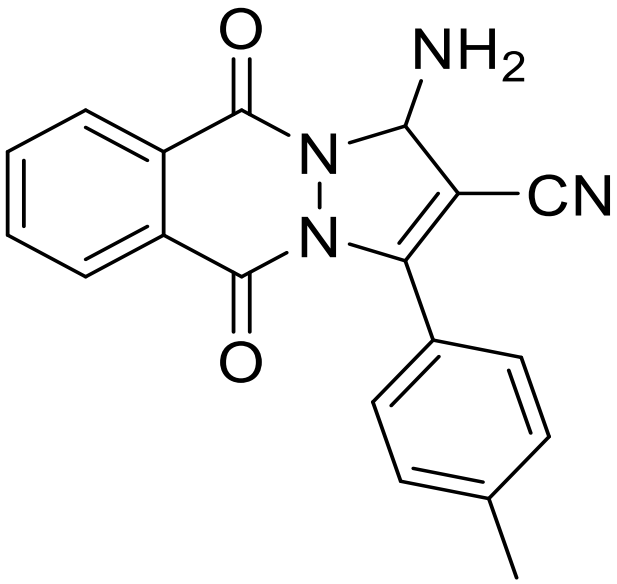

Py-3

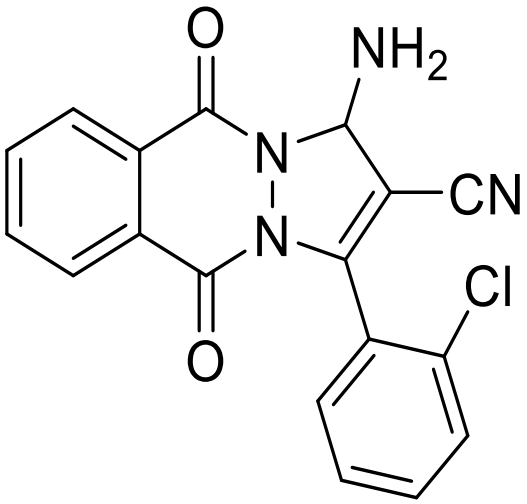

Py-4

Figure 1. Chemical structure of the investigated v: **Py-3** and **Py-4**

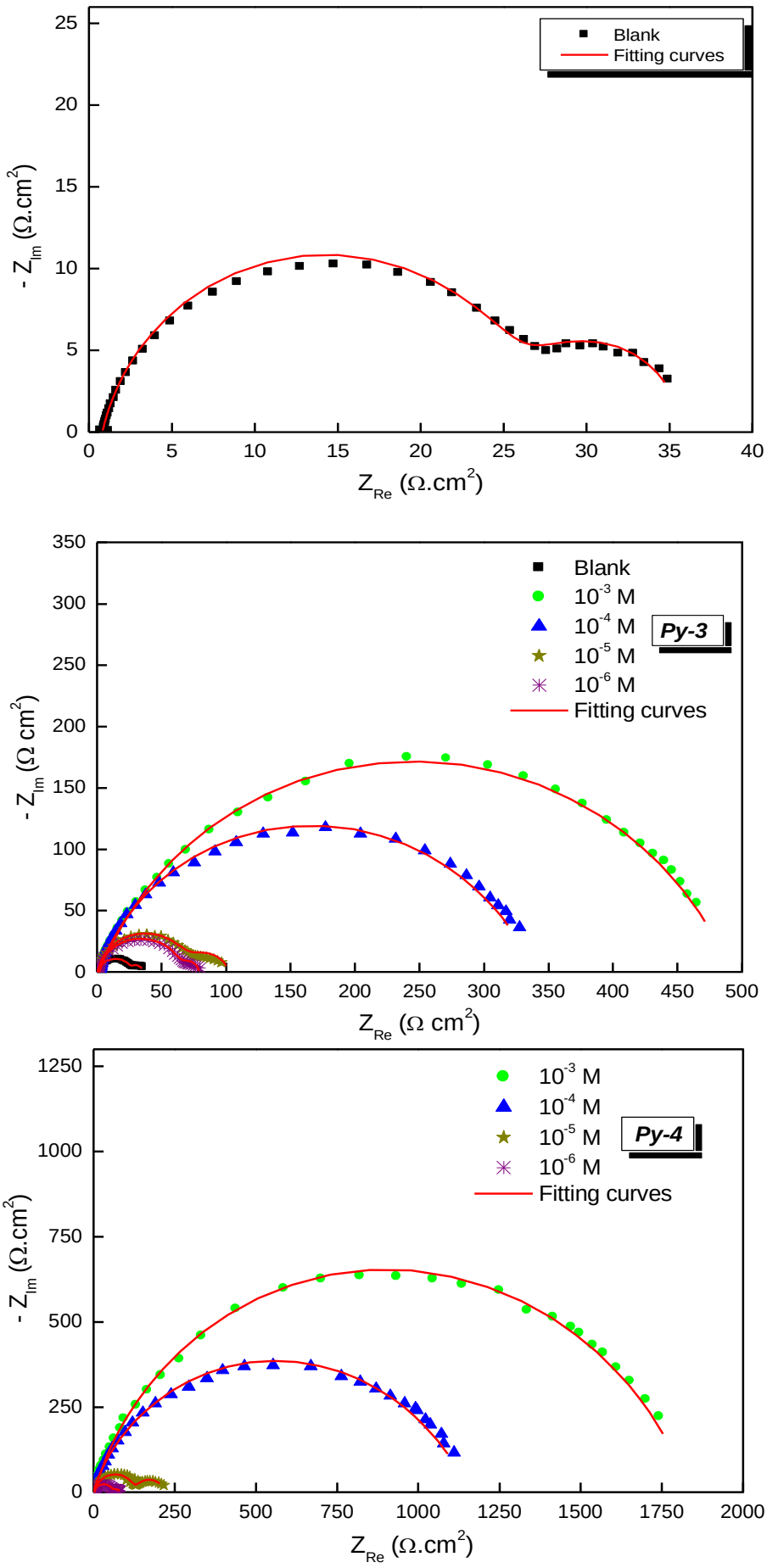

Figure 2. Nyquist plot of stainless steel in 2M H_2SO_4 solution with and without different concentrations of Py-3 and Py-4

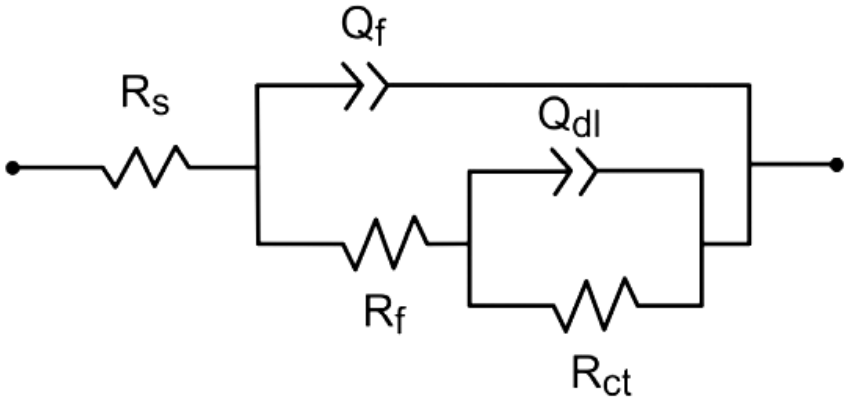

Figure 3. Equivalent circuit used to model the impedance diagrams

Table 2. Electrochemical impedance parameters in the absence and presence of inhibitors at different concentrations

Conc. M	R_s Ω cm²	Q_f µFcm²	n_f	R_f Ω cm²	Q_{tc} µF cm²	n_{tc}	R_{tc} Ω cm²	R_p Ω cm²	η_{imp}%	θ
H_2SO_4 2M										
--	0.8	958	0.864	26.8	625	1	8.1	34,9	--	--
Py-3										
10^{-6}	0.7	673	0.875	66.4	433	0.984	15.0	81,4	**57,1**	0.571
10^{-5}	0.6	511	0.910	72.0	406	0.858	29.4	101,4	**65,6**	0.656
10^{-4}	2.0	162	0.934	23.0	391	0.664	315.3	338,3	**89,7**	0.897
10^{-3}	1.5	185	0.895	37.3	356	0.696	453.2	490,5	**92,9**	0.929
Py-4										
10^{-6}	0.9	698.7	0.878	57.2	613	0.729	23.0	80,2	**56,5**	0.565
10^{-5}	0.8	522.3	0.865	128.8	576	0.844	88.2	217	**83,9**	0.839
10^{-4}	0.6	60.6	0.999	40.7	341	0.688	1155	1195,7	**97,1**	0.971
10^{-3}	0.7	90.8	0.950	40.5	216	0.706	1803	1843,5	**98,1**	0.981

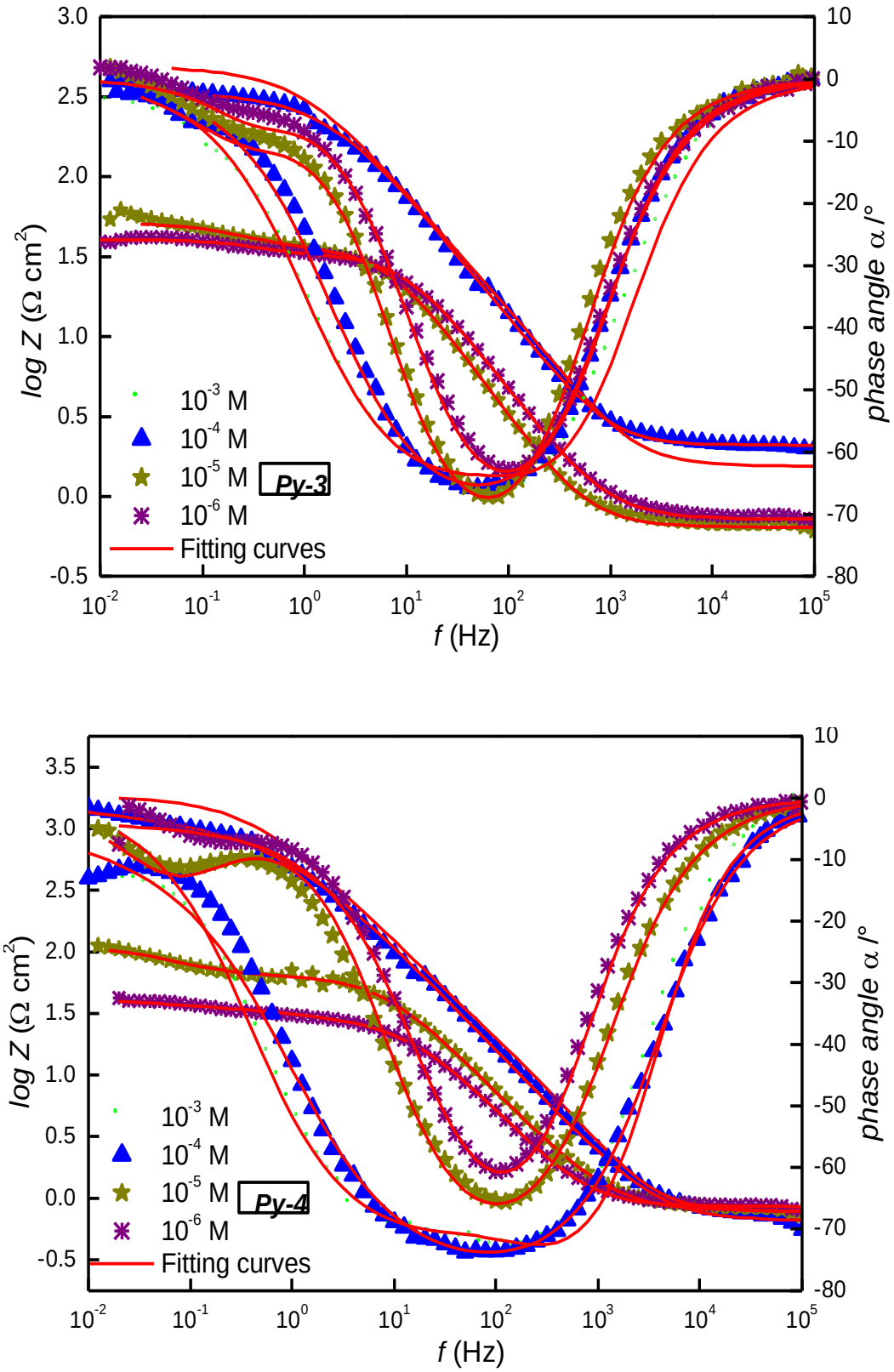

Figure 4. Bode plots of the steel in a 2M H_2SO_4 solution in the absence and presence of inhibitors at various concentrations.

Table 3. Adsorption isotherm models

Isotherme	*Forme linéaire*	*Courbe*	*Réf*
Langmuir	$k_{ads}C_{inh} = \frac{\theta}{1-\theta}$	$\frac{C_{inh}}{\theta} = f(C_{inh})$	**[48]**
Freundlich	$\theta = K_{ads}C_{inh}^{n}$	$ln\theta = f(lnC_{inh})$	**[49]**
Temkin	$e^{-2f\theta} = k_{ads}C_{inh}$	$\theta = f(lnC_{inh})$	**[50]**
Flory-Higgins	$\frac{\theta}{c_{inh}} = k_{ads}(1-\theta)^{a}$	$ln\frac{\theta}{C_{inh}} = f(ln1-\theta)$	**[51,52]**
Frumkin	$\frac{\theta}{1-\theta}e^{-2f\theta} = k_{ads}C_{inh}$	$ln\left(C_{inh}\frac{1-\theta}{\theta}\right) = f(\theta)$	**[53]**
El-Aawady	$\left(\frac{\theta}{1-\theta}\right)^{1/\gamma} = k_{ads}C_{inh}$	$ln(1-\theta) = fln\left(\frac{\theta}{C_{inh}}\right)$	**[54]**

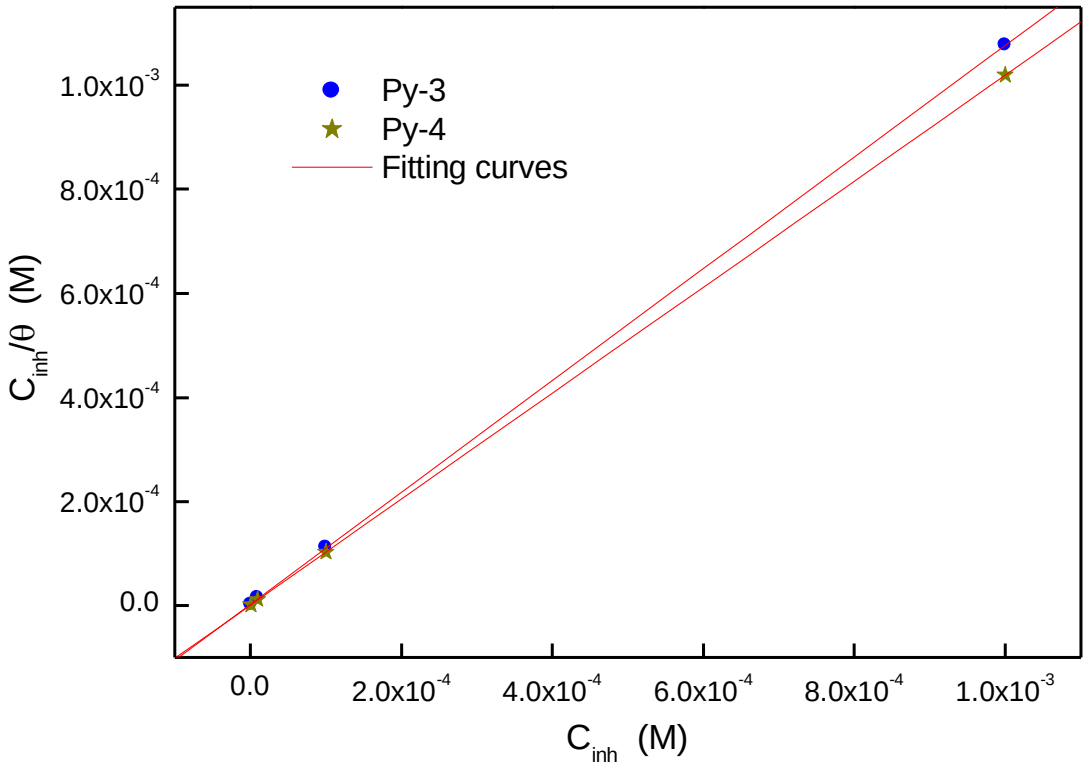

Figure 5. Langmuir adsorption isotherm of Py-3 and Py-4 on the surface of stainless steel at 298K.

Table 4. Thermodynamic parameters for inhibitor adsorption on steel at 298K.

K_{ads} (L/mol)	ΔG_{ads} (Kj/mol)	R^2	Slopes
Py-3			
32.6 10^4	-41.4	0,99999	1,07
Py-4			
81.910^4	-43.6	1	1,02

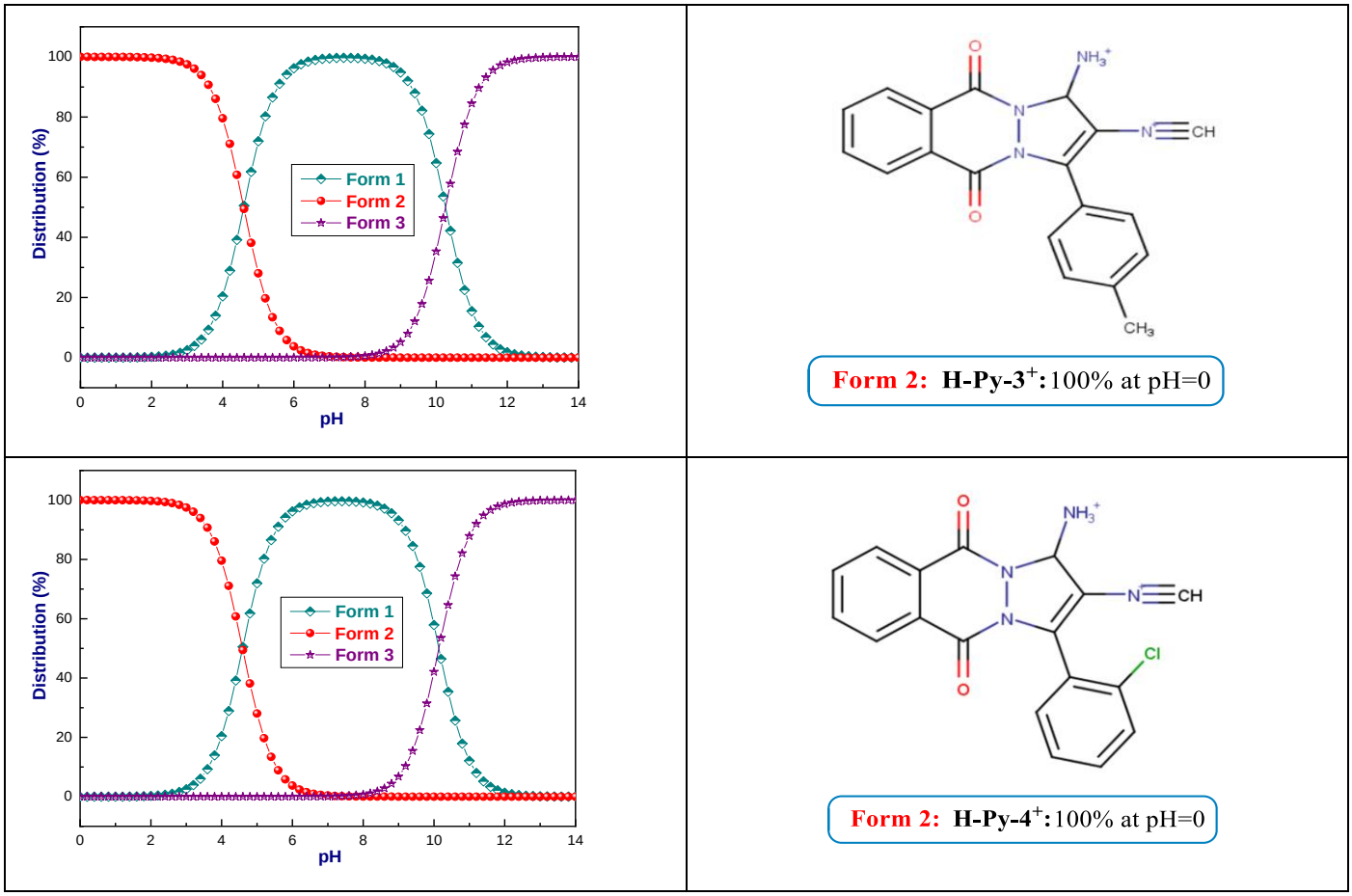

Figure 6. Percentage of species observed as a function of the pH diagrams of the molecules studied using MarvinSketch software

Table 5. Quantum chemical descriptors calculated for neutral and protonated forms at the B3LYP/6–311G (d,p) basis set in aqueous phase

Parameter	Py-3	Py-4	H-Py-3$^+$	H-Py-4$^+$
E_{HOMO} (eV)	-6,285	-6,363	-6,860	-7,049
E_{LUMO} (eV)	-2,387	-2,409	-2,906	-2,934
ΔE_{gap} (eV)	3,897	3,954	3,954	4,114
η (eV)	1,948	1,977	1,977	2,057
σ (eV)	0,513	0,505	0,505	0,486
χ(eV)	4,336	4,386	4,883	4,991
ΔN	0,124	0,109	-0,0161	-0,041

Forms	Structures optimizes	HOMOs	LUMOs	MEPs
Py-3	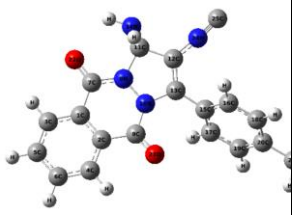	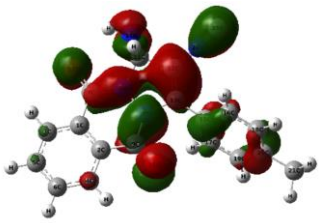	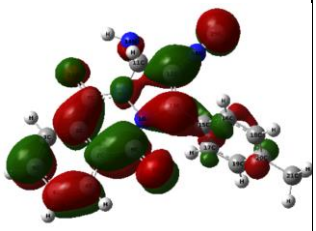	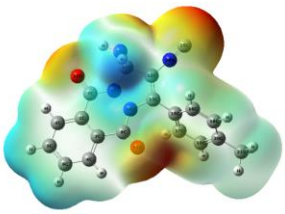
Py-4	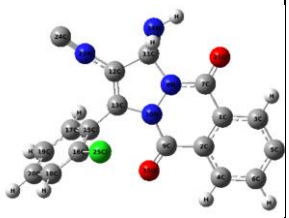	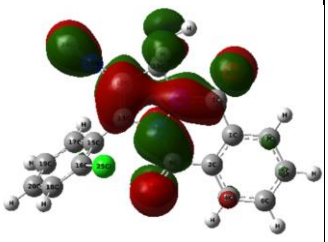	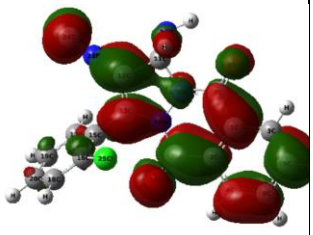	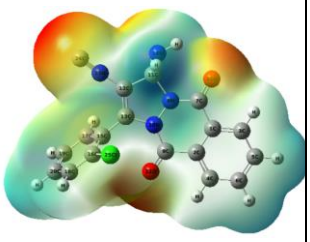
H-Py-3^{+}	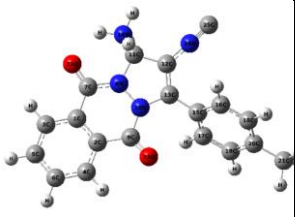	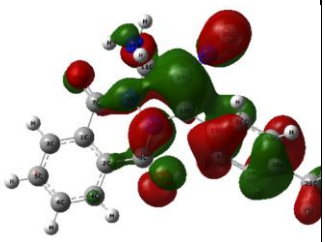	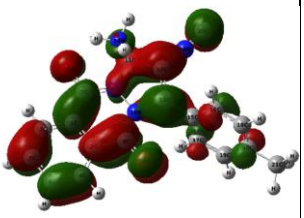	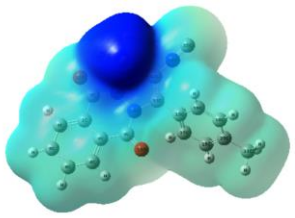
H-Py-4^{+}	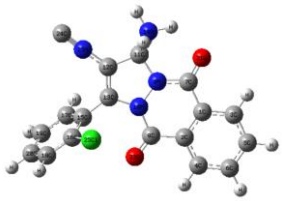	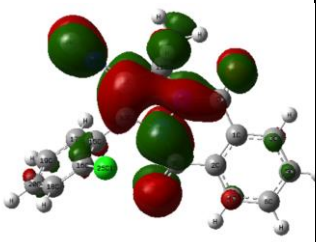	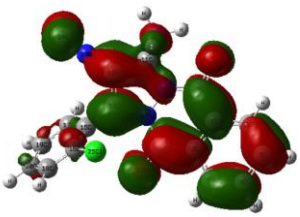	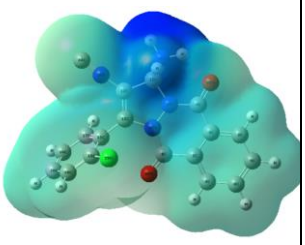

Figure 7. Optimized structures and distribution of electron density on the HOMO and LUMO orbitals of the neutral and protonated forms of the inhibitors studied at the DFT/B3LYP6–311G (d,p) basis set

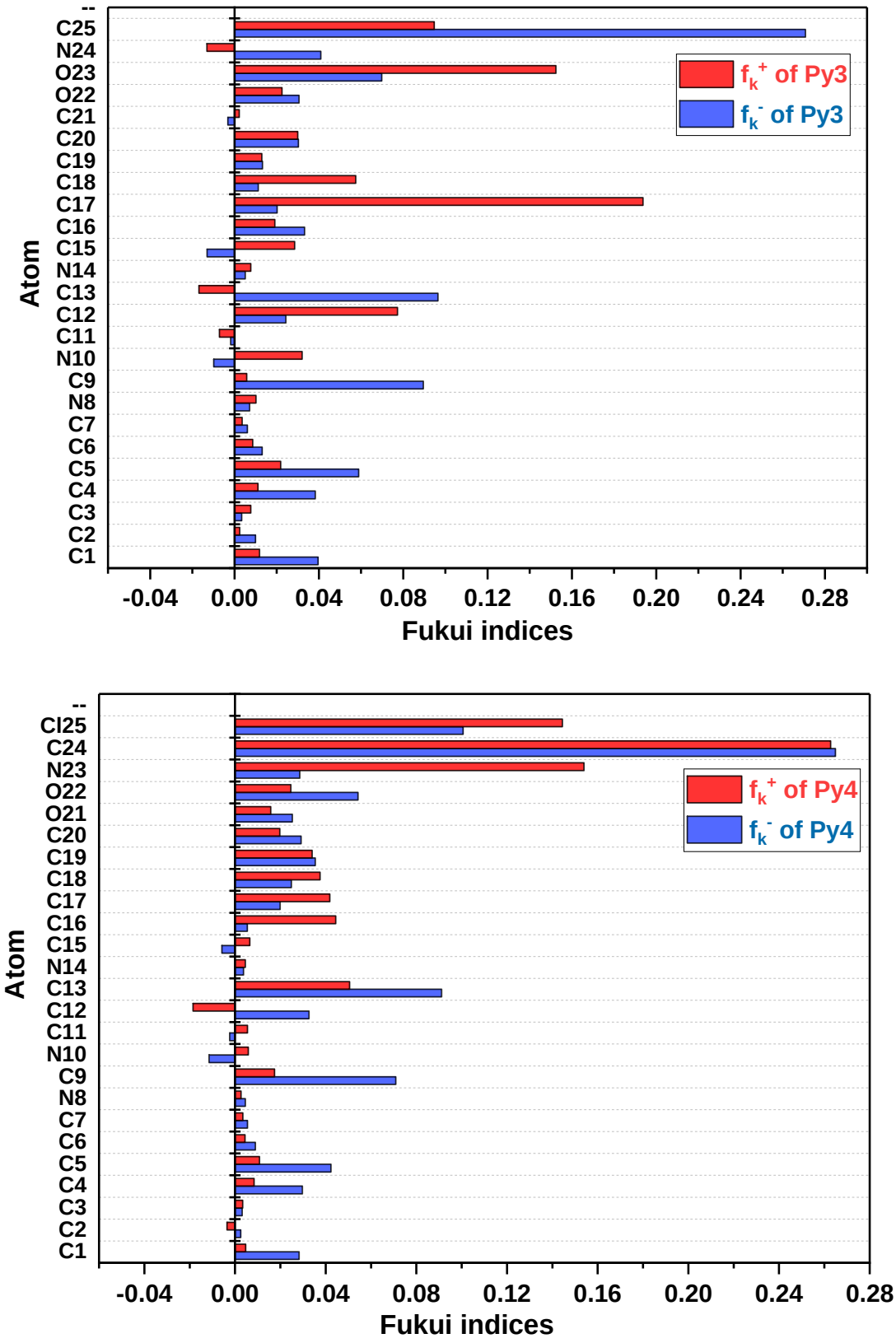

Figure 8. Graphical representations of the calculated Fukui index for the molecules studied in aqueous solution

4. Conclusions

This work has shown that the two organic molecules are excellent inhibitors for steel in acid media, even at very low concentrations. The Py-4 compound is regarded as the most effective inhibitor, with an inhibitory efficiency of 98.1%. Furthermore, the variation of C/θ with the concentration of our inhibitors indicates that their adsorption on the metal surface follows the Langmuir isotherm model. The standard free energy of adsorption ΔG_{ads} calculated for the both inhibitors indicates that the adsorption of our inhibitors on the steel surface is chemical type. On the other hand, the quantum chemical calculations give a better overview on the reactivity of tested inhibitor towards stainless steel which they are in good agreement with the experimental findings. Fukui indices revealed that the most probable sites for electrophilic and nucleophilic attacks are the regions of the pyrazolo-pyridazine fraction, the chlorine atoms, as well as the various nitrogen and oxygen heteroatoms.

References

[1] Y. Fernine, N. Arrousse, R. Haldhar, C.J. Raorane, E. Ech-Chihbi, S.C. Kim, M. Taleb. (2022). Novel thiophene derivatives as eco-friendly corrosion inhibitors for mild steel in 1 M HCl solution: Characterization, electrochemical and computational (DFT and MC simulations) methods. Journal of Environmental Chemical Engineering. 10 (6) 108891.

[2] K.E. Mouaden, D.S. Chauhan, M.A. Quraishi, L. Bazzi. (2020). Thiocarbohydrazide-crosslinked chitosan as a bioinspired corrosion inhibitor for protection of stainless steel in 3.5% NaCl. Sustainable chemistry and pharmacy. 15 100213.

[3] C.L. Wang, H.D. Guo, J. Fang, S.X. Yu, X.Q. Yue, Q.H. Hu, Y.X. Li. (2023). The role of Cr content on the corrosion resistance of carbon steel and low-Cr steels in the CO2-saturated brine. Petroleum Science. 20 (2) 1155-1168.

[4] P.C. Chiang, C.W. Chen, F.T. Tsai, C.K. Lin, C.C. Chen. (2021). Hard anodization film on carbon steel surface by thermal spray and anodization methods. Materials. 14 (13) 3580.

[5] K. Hoshino, S. Furuya, R.G. Buchheit. (2018). Effect of NO_3− intercalation on corrosion resistance of conversion coated Zn-Al-CO_3 LDHs on electrogalvanized steel. Journal of The Electrochemical Society. 165 (9) C461.

[6] H. Guo, C. Zhu, Z. Yuan, G. Huang, H. Liang, C. Xiong, G. Meng. (2023). Facile Hydrogels of AIEgens Applied as Reusable Sensors for In Situ and Early Warning of Metallic Corrosion. ACS Applied Materials & Interfaces. 15 (6) 8530-8536.

[7] E. McCafferty. (2010). Introduction to corrosion science. Springer Science & Business Media.

[8] W. Kautek. (1988). The galvanic corrosion of steel coatings: aluminum in comparison to cadmium and zinc. Corrosion science. 28 (2) 173-199.

[9] M. Ouakki, M. Galai, M. Rbaa, A.S. Abousalem, B. Lakhrissi, E.H. Rifi, M. Cherkaoui. (2019). Quantum chemical and experimental evaluation of the inhibitory action of two imidazole derivatives on mild steel corrosion in sulphuric acid medium. Heliyon. 5 (11) e02759.

[10] M. Ouakki, M. Galai, M. Cherkaoui. (2022). Imidazole derivatives as efficient and potential class of corrosion inhibitors for metals and alloys in aqueous electrolytes: A review. Journal of Molecular Liquids. 345 117815.

[11] K. Dahmani, M. Galai, M. Ouakki, M. Cherkaoui, R. Touir, S.U.L.T.A.N. Erkan, B. El Ibrahimi. (2021). Quantum chemical and molecular dynamic simulation studies for the identification of the extracted cinnamon essential oil constituent responsible for copper corrosion inhibition in acidified 3.0 wt% NaCl medium. Inorganic Chemistry Communications. 124 108409.

[12] M. Ouakki, M. Galai, Z. Aribou, Z. Benzekri, K. Dahmani, E. Ech-chihbi, M. Cherkaoui. (2022). Detailed experimental and computational explorations of pyran derivatives as corrosion inhibitors for mild steel in 1.0 M HCl: Electrochemical/surface studies, DFT modeling, and MC simulation. Journal of Molecular Structure. 1261 132784.

[13] M. Ouakki, M. Galai, M. Rbaa, A.S. Abousalem, B. Lakhrissi, E.H. Rifi, M. Cherkaoui. (2020). Investigation of imidazole derivatives as corrosion inhibitors for mild steel in sulfuric acidic environment: experimental and theoretical studies. Ionics. 26 (10) 5251-5272.

[14] M. ElBelghiti, Y. Karzazi, A. Dafali, B. Hammouti, F. Bentiss, I.B. Obot, E.E. Ebenso. (2016). Experimental, quantum chemical and Monte Carlo simulation studies of 3, 5-disubstituted-4-amino-1, 2, 4-triazoles as corrosion inhibitors on mild steel in acidic medium. Journal of Molecular Liquids. 218 281-293.

[15] A. Zarrouk, B. Hammouti, T. Lakhlifi, M. Traisnel, H. Vezin, F. Bentiss. (2015). New 1H-pyrrole-2, 5-dione derivatives as efficient organic inhibitors of carbon steel corrosion in hydrochloric acid medium: electrochemical, XPS and DFT studies. Corrosion Science. 90 572-584.

[16] K. Cherrak, F. Benhiba, N.K. Sebbar, E.M. Essassi, M. Taleb, A. Zarrouk, A. Dafali. (2019). Corrosion inhibition of mild steel by new Benzothiazine derivative in a hydrochloric acid solution: Experimental evaluation and theoretical calculations. Chemical Data Collections. 22 100252.

[17] M. El Azzouzi, A. Aouniti, S. Tighadouin, H. Elmsellem, S. Radi, B. Hammouti, A. Zarrouk. (2016). Some hydrazine derivatives as corrosion inhibitors for mild steel in 1.0 M HCl: weight loss, electrochemichal, SEM and theoretical studies. Journal of Molecular Liquids. 221 633-641.

[18] C. Verma, V.S. Saji, M.A. Quraishi, E.E. Ebenso. (2020). Pyrazole derivatives as environmental benign acid corrosion inhibitors for mild steel: Experimental and computational studies. Journal of Molecular Liquids. 298 111943.

[19] I. Selatnia, A. Sid, M. Benahmed, O. Dammene debbih, T. Ozturk, N. Gherraf. (2018). Synthesis and

characterization of a bis-pyrazoline derivative as corrosion inhibitor for A283 carbon steel in 1M HCl: electrochemical, surface, DFT and MD simulation studies. Protection of Metals and Physical Chemistry of Surfaces. 54 1182-1193.

[20] C.R. Prokopp, M.A. Rubin, P.D. Sauzem, A.H. De Souza, D.B. Berlese, R.V. Lourega, C.F. Mello. (2006). A pyrazolyl-thiazole derivative causes antinociception in mice. Brazilian journal of medical and biological research. 39 795-799.

[21] M.J. Naim, O. Alam, F. Nawaz, M.J. Alam, P. Alam. (2016). Current status of pyrazole and its biological activities. Journal of Pharmacy and Bioallied Sciences. 8 (1) 2-17.

[22] M. El Faydy, B. Lakhrissi, A. Guenbour, S.A.V.A.S. Kaya, F. Bentiss, I. Warad, A. Zarrouk. (2019). In situ synthesis, electrochemical, surface morphological, UV–visible, DFT and Monte Carlo simulations of novel 5-substituted-8-hydroxyquinoline for corrosion protection of carbon steel in a hydrochloric acid solution. Journal of Molecular Liquids. 280 341-359.

[23] F. Bentiss, M. Outirite, M. Traisnel, H. Vezin, M. Lagrenée, B. Hammouti, C. Jama. (2012). Improvement of corrosion resistance of carbon steel in hydrochloric acid medium by 3, 6-bis (3-pyridyl) pyridazine. International Journal of Electrochemical Science. 7 (2) 1699-1723.

[24] M. El Achouri, M.R. Infante, F. Izquierdo, S. Kertit, H.M. Gouttaya, B. Nciri. (2001). Synthesis of some cationic gemini surfactants and their inhibitive effect on iron corrosion in hydrochloric acid medium. Corrosion Science. 43 (1) 19-35.

[25] B. AitHaddou, D. Chebabe, A. Dermaj, H. Benassaoui, A. El Assyry, N. Hajjaji, A. Srhiri. (2016). Comparative study of low carbon steel corrosion inhibition in 1M HCl by 1, 2, 4-triazole-5-thione derivatives. J. Mater. Environ. Sci. 7 (6) 2191-12000.

[26] A.O. Yüce, G. Kardaş. (2012). Adsorption and inhibition effect of 2-thiohydantoin on mild steel corrosion in 0.1 M HCl. Corrosion Science. 58 86-94.

[27] S. Martinez, M. Metikoš-Huković. (2003). A nonlinear kinetic model introduced for the corrosion inhibitive properties of some organic inhibitors. Journal of Applied Electrochemistry. 33 1137-1142.

[28] M. Elayyachy, A. El Idrissi, B. Hammouti. (2006). New thio-compounds as corrosion inhibitor for steel in 1 M HCl. Corrosion Science. 48 (9) 2470-2479.

[29] F. Mansfeld. (1981). Recording and analysis of AC impedance data for corrosion studies. Corrosion. 37 (5) 301-307.

[30] X. Zheng, S. Zhang, M. Gong, W. Li. (2014). Experimental and theoretical study on the corrosion inhibition of mild steel by 1-octyl-3-methylimidazolium L-prolinate in sulfuric acid solution. Industrial & engineering chemistry research. 53 (42) 16349-16358.

[31] M.T. Saeed, M. Saleem, S. Usmani, I.A. Malik, F.A. Al-Shammari, K.M. Deen. (2019). Corrosion inhibition of mild steel in 1 M HCl by sweet melon peel extract. Journal of King Saud University-Science. 31 (4) 1344-1351.

[32] S.S.A. Rehim, H.H. Hassan, M.A. Amin. (2002). Corrosion and corrosion inhibition of Al and some alloys in sulphate solutions containing halide ions investigated by an impedance technique. Applied Surface Science. 187 (3-4) 279-290.

[33] H. Zarrok, A. Zarrouk, B. Hammouti, R. Salghi, C. Jama, F.J.C.S. Bentiss. (2012). Corrosion control of carbon steel in phosphoric acid by purpald–Weight loss, electrochemical and XPS studies. Corrosion Science. 64 243-252.

[34] H. Ouici, M. Tourabi, O. Benali, C. Selles, C. Jama, A. Zarrouk, F. Bentiss. (2017). Adsorption and corrosion inhibition properties of 5-amino 1, 3, 4-thiadiazole-2-thiol on the mild steel in hydrochloric acid medium: Thermodynamic, surface and electrochemical studies. Journal of Electroanalytical Chemistry. 803 125-134.

[35] M. Rbaa, F. Benhiba, A.S. Abousalem, M. Galai, Z. Rouifi, H. Oudda, A. Zarrouk. (2020). Sample synthesis, characterization, experimental and theoretical study of the inhibitory power of new 8-hydroxyquinoline derivatives for mild steel in 1.0 M HCl. Journal of Molecular Structure. 1213 128155.

[36] M. Behpour, S.M. Ghoreishi, N. Soltani, M. Salavati-Niasari, M. Hamadanian, A. Gandomi. (2008). Electrochemical and theoretical investigation on the corrosion inhibition of mild steel by thiosalicylaldehyde derivatives in hydrochloric acid solution. Corrosion Science. 50 (8) 2172-2181.

[37] A.K. Singh, M.A. Quraishi. (2009). Effect of 2, 2′ benzothiazolyl disulfide on the corrosion of mild steel in acid media. Corrosion science. 51 (11) 2752-2760.

[38] J. Aljourani, K. Raeissi, M.A. Golozar. (2009). Benzimidazole and its derivatives as corrosion inhibitors for mild steel in 1M HCl solution. Corrosion science. 51 (8) 1836-1843.

[39] H.M. Abd El-Lateef. (2016). Synergistic effect of polyethylene glycols and rare earth Ce 4+ on the corrosion inhibition of carbon steel in sulfuric acid solution: Electrochemical, computational, and surface morphology studies. Research on Chemical Intermediates. 42 3219-3240.

[40] C.H. Hsu, F. Mansfeld. (2001). Concerning the conversion of the constant phase element parameter Y0 into a capacitance. Corrosion. 57 (09).

[41] M. El Faydy, M. Galai, M. Rbaa, M. Ouakki, B. Lakhrissi, M.E. Touhami, Y. El Kacimi. (2018). Synthesis and application of new quinoline as hydrochloric acid corrosion inhibitor of carbon steel. Anal. Bioanal. Electrochem. 10 (7) 815-839.

[42] H. Tian, W. Li, B. Hou. (2011). Novel application of a hormone biosynthetic inhibitor for the corrosion resistance enhancement of copper in synthetic seawater. Corrosion Science. 53 (10) 3435-3445.

[43] H. Tian, W. Li, K. Cao, B. Hou. (2013). Potent inhibition of copper corrosion in neutral chloride media by novel non-toxic thiadiazole derivatives. Corrosion science. 73 281-291.

[44] K. Chkirate, K. Azgaou, H. Elmsellem, B. El Ibrahimi, N.K. Sebbar, M. Benmessaoud, E.M. Essassi. (2021). Corrosion inhibition potential of 2-[(5-methylpyrazol-3-yl) methyl] benzimidazole against carbon steel corrosion in 1 M HCl solution: Combining experimental and theoretical studies. Journal of Molecular Liquids. 321 114750.

[45] D.K. Yadav, M.A. Quraishi. (2012). Application of some condensed uracils as corrosion inhibitors for mild steel: gravimetric, electrochemical, surface morphological, UV–visible, and theoretical investigations. Industrial & engineering chemistry research. 51 (46) 14966-14979.

[46] B. Rikhari, S.P. Mani, N. Rajendran. (2016). Investigation of corrosion behavior of polypyrrole-coated Ti using dynamic electrochemical impedance spectroscopy (DEIS). RSC Advances. 6 (83) 80275-80285.

[47] A. Boutouil, M.R. Laamari, I. Elazhary, L. Bahsis, H. Anane, S.E Stiriba. (2020). Towards a deeper understanding of the inhibition mechanism of a new 1, 2, 3-triazole derivative for mild steel corrosion in the hydrochloric acid solution using coupled experimental and theoretical methods. Materials Chemistry and Physics. 241 122420.

[48] I. Langmuir. (1916). The constitution and fundamental properties of solids and liquids. Part I. Solids. Journal of the American chemical society. 38 (11) 2221-2295.

[49] C.H. Yang. (1998). Statistical mechanical study on the Freundlich isotherm equation. Journal of colloid and interface science. 208 (2) 379-387.

[50] M.J. Temkin, V. Pyzhev. (1940). Recent modifications to Langmuir isotherms.

[51] M.H. Jnr, A.I. Spiff. (2005). Equilibrium sorption study of Al^{3+}, Co^{2+} and Ag^{+} in aqueous solutions by fluted pumpkin (Telfairia occidentalis HOOK f) waste biomass. Acta Chim. Slov. 52 174-181.

[52] J. Derco, B. Vrana (Eds.). (2018). Biosorption. BoD–Books on Demand.

[53] A. Frumkin. (1925). Die Kapillarkurve der höheren Fettsäuren und die Zustandsgleichung der Oberflächenschicht. Zeitschrift für Physikalische Chemie. 116 (1) 466-484.

[54] A.A. El-Awady, B.A. Abd-El-Nabey, S.G. Aziz. (1992). Kinetic-thermodynamic and adsorption isotherms analyses for the inhibition of the acid corrosion of steel by cyclic and open-chain amines. Journal of the Electrochemical Society. 139 (8) 2149.

[55] R.J. Chin, K. Nobe. (1971). Electrochemical characteristics of iron in H 2 SO 4 containing benzotriazole. Journal of the Electrochemical Society. 118 (4) 545.

[56] D.K. Verma, S. Kaya, E. Ech-chihbi, F. El-Hajjaji, M.M. Phukan, H.M. Alnashiri. (2021). Investigations on some coumarin based corrosion inhibitors for mild steel in aqueous acidic medium: Electrochemical, surface morphological, density functional theory and Monte Carlo simulation approach. Journal of Molecular Liquids. 329 115531.

[57] P. Mourya, S. Banerjee, M.M. Singh. (2014). Corrosion inhibition of mild steel in acidic solution by Tagetes erecta (Marigold flower) extract as a green inhibitor. Corrosion Science. 85 352-363.

[58] F.M. Donahue, K. Nobe. (1965). Theory of organic corrosion inhibitors: adsorption and linear free energy relationships. Journal of the Electrochemical Society. 112 (9) 886.

[59] E. Khamis, F. Bellucci, R.M. Latanision, E.S.H. El-Ashry. (1991). Acid corrosion inhibition of nickel by 2-(triphenosphoranylidene) succinic anhydride. Corrosion. 47 (9) 677-686.

[60] A. Tazouti, M. Galai, R. Touir, M.E. Touhami, A. Zarrouk, Y. Ramli, C. Kaya. (2016). Experimental and theoretical studies for mild steel corrosion inhibition in 1.0 M HCl by three new quinoxalinone derivatives. Journal of Molecular Liquids. 221 815-832.

[61] M. ElBelghiti, Y. Karzazi, A. Dafali, B. Hammouti, F. Bentiss, I.B. Obot, E.E. Ebenso. (2016). Experimental, quantum chemical and Monte Carlo simulation studies of 3, 5-disubstituted-4-amino-1, 2, 4-triazoles as corrosion inhibitors on mild steel in acidic medium. Journal of Molecular Liquids. 218 281-293.

[62] J.R. Cheeseman, M.J. Frisch. (2011). Basis set dependence of vibrational Raman and Raman optical activity intensities. Journal of Chemical Theory and Computation. 7 (10) 3323-3334.

[63] M. Galai, M. Rbaa, M. Ouakki, A.S. Abousalem, E. Ech-Chihbi, K. Dahmani, M. Ebn Touhami. (2020). Chemically functionalized of 8-hydroxyquinoline derivatives as efficient corrosion inhibition for steel in 1.0 M HCl solution: Experimental and theoretical studies. Surfaces and Interfaces. 21 100695.

[64] M. Missioui, M.B. Idrissi, F. Benhiba, Z. Atioğlu, M. Akkurt, H. Oudda, Y. Ramli. (2022). Synthesis, structural characterization, Hirshfeld surface analysis and anti-corrosion on mild steel in 1M HCl of ethyl 2-(3-methyl-2-oxo-1, 2-dihydroquinoxaline-1-yl) acetate. Journal of Molecular Structure. 1251 132047.

[65] M.A. Deyab, S.S. Abd El-Rehim. (2013). Influence of polyethylene glycols on the corrosion inhibition of carbon steel in butyric acid solution: weight loss, EIS and theoretical studies. International Journal of Electrochemical Science. 8 (12) 12613-12627.

[66] F.E. kalai, T. Chelfi, N. Benchat, M. Bouklah, S. Daoui, K. Karrouchi, T. Ben Hadda. (2020). New heterocyclic compounds based on pyridazinones scaffold as efficient inhibitor of corrosion of mild steel in acidic solution 1 M HCl. Journal of Bio-and Tribo-Corrosion. 6 1-14.

[67] M. Ouakki, M. Galai, M. Rbaa, A.S. Abousalem, B. Lakhrissi, M.E. Touhami, M. Cherkaoui. (2020). Electrochemical, thermodynamic and theoretical studies of some imidazole derivatives compounds as acid corrosion inhibitors for mild steel. Journal of Molecular Liquids. 319 114063.

[68] M. Saraçoğlu, M.I.A. Elusta, S. Kaya, C. Kaya, F. Kandemirli. (2018). Quantum chemical studies on the corrosion inhibition of Fe78B13Si9 glassy alloy in Na2SO4 solution of some thiosemicarbazone

derivatives. International Journal of Electrochemical Science. 13 (8) 8241-8259.

[69] S.K. Saha, P. Banerjee. (2015). A theoretical approach to understand the inhibition mechanism of steel corrosion with two aminobenzonitrile inhibitors. RSC advances. 5 (87) 71120-71130.

[70] P.K. Paul, M. Yadav, I.B. Obot. (2020). Investigation on corrosion protection behavior and adsorption of carbohydrazide-pyrazole compounds on mild steel in 15% HCl solution: Electrochemical and computational approach. Journal of Molecular Liquids. 314 113513.

[71] E. Ech-Chihbi, M.E. Belghiti, R. Salim, H. Oudda, M. Taleb, N. Benchat, F. El-Hajjaji. (2017). Experimental and computational studies on the inhibition performance of the organic compound "2-phenylimidazo [1, 2-a] pyrimidine-3-carbaldehyde" against the corrosion of carbon steel in 1.0 M HCl solution. Surfaces and Interfaces. 9 206-217.

[72] I.B. Obot, D.D. Macdonald, Z.M. Gasem. (2015). Density functional theory (DFT) as a powerful tool for designing new organic corrosion inhibitors. Part 1: an overview. Corrosion Science. 99 1-30.

[73] E. Ech-Chihbi, A. Nahlé, R. Salim, F. Benhiba, A. Moussaif, F. El-Hajjaji, A. Zarrouk. (2020). Computational, MD simulation, SEM/EDX and experimental studies for understanding adsorption of benzimidazole derivatives as corrosion inhibitors in 1.0 M HCl solution. Journal of Alloys and Compounds. 844 155842.

[74] F. El-Hajjaji, E. Ech-Chihbi, N. Rezki, F. Benhiba, M. Taleb, D.S. Chauhan, M.A. Quraishi. (2020). Electrochemical and theoretical insights on the adsorption and corrosion inhibition of novel pyridinium-derived ionic liquids for mild steel in 1 M HCl. Journal of Molecular Liquids. 314 113737.